Since January 2020 Elsevier has created a COVID-19 resource centre with free information in English and Mandarin on the novel coronavirus COVID-19. The COVID-19 resource centre is hosted on Elsevier Connect, the company's public news and information website.

Journal of Molecular Liquids 345 (2022) 117852

Contents lists available at ScienceDirect

Journal of Molecular Liquids

journal homepage: www.elsevier.com/locate/molliq

A molecular dynamic study on the ability of phosphorene for designing new sensor for SARS-CoV-2 detection

Aliyeh Mehranfar [a], Mohammad Khavani [b], Mohammad Izadyar [a,*]

[a] Research Center for Modeling and Computational Sciences, Department of Chemistry, Faculty of Science, Ferdowsi University of Mashhad, Mashhad, Iran
[b] Department of Chemistry and Materials Science, School of Chemical Engineering, Aalto University, P.O. Box 16100, FI-00076 Aalto, Finland

ARTICLE INFO

Article history:
Received 29 September 2021
Revised 11 October 2021
Accepted 13 October 2021
Available online 16 October 2021

Keywords:
Coronavirus
MD simulation
Sensor
Electrostatic interaction
Nanostructures
Graphene
Phosphorene

ABSTRACT

Due to the dramatic increase in the number of patients with severe acute respiratory syndrome coronavirus 2 (SARS-CoV-2), designing new selective and sensitive sensors for the detection of this virus is of importance. In this research, by employing full atomistic molecular dynamics (MD) simulations, the interactions of the receptor-binding domain (RBD) of the SARS-CoV-2 with phosphorene and graphene nanosheets were analyzed to investigate their sensing ability against this protein. Based on the obtained results, the RBD interactions with the surface of graphene and phosphorene nanosheets do not have important effects on the folding properties of the RBD but this protein has unique dynamical behavior against each nanostructure. In the presence of graphene and phosphorene, the RBD has lower stability because due to the strong interactions between RBD and these nanostructures. This protein spreads on the surface and has lower structural compaction, but in comparison with graphene, RBD shows greater stability on the surface of the phosphorene nanosheet. Moreover, RBD forms a more stable complex with phosphorene nanosheet in comparison with graphene due to greater electrostatic and van der Waals interactions. The calculated Gibbs binding energy for the RBD complexation process with phosphorene and graphene are −200.37 and −83.65 kcal mol^{-1}, respectively confirming that phosphorene has higher affinity and sensitivity against this protein than graphene. Overall, the obtained results confirm that phosphorene can be a good candidate for designing new nanomaterials for selective detection of SARS-CoV-2.

1. Introduction

At the moment, the novel coronavirus disease (COVID-19) leads to severe acute respiratory syndrome coronavirus 2 (SARS-CoV-2), which is one of the most important challenges that the world is facing [1–4]. This virus has different types that can infect mammalian animals and humans [5,6]. The alpha and beta species can infect humans and cause serious health problems [7]. The phylogenic analysis confirmed that the novel coronavirus belongs to the β-coronavirus family similar to the other beta coronaviruses such as Middle East respiratory syndrome coronavirus (MERS-CoV), bat-SARS coronavirus, and SARS-CoV [8–10]. The SARS-CoV-2 is composed of four proteins, including M (Membrane), S (Spike), E (Envelope), and N (Nucleocapsid) proteins [11]. The coronavirus can enter into the host cell through a mechanism of receptor binding followed by a fusion of viral and host membranes [12]. The spike protein of the coronavirus is composed of S1 and S2 subunits. The receptor-binding-domain (RBD) of S1 protein interacts with angiotensin-converting enzyme 2 (ACE2) as the host cellular receptor [13–15].

There are many experimental and theoretical reports in the literature about drug design on antiviral agents against coronavirus and structural studies on this virus. Since the structure of the SARS-CoV-2 is similar to SARS-CoV (79.5 % of sequence similarity), Xu and et al. reported that niclosamide can be used as an effective antiviral agent against the novel coronavirus [16]. Moreover, theoretical studies revealed that ritonavir and lopinavir drugs have considerable potential for use as inhibitors for SARS-CoV-2 [17]. Based on the computational results, ritonavir has more inhibitory effects against coronavirus in comparison with lopinavir due to greater van der Waals (vdW) and electrostatic interactions with the active site of the novel coronavirus [17]. The ability of eravacycline, valrubicin, carfilzomib, and elbasvir were investigated by applying theoretical methods by Wang and coworkers [18]. Based on the obtained results, carfilzomib shows better outcomes for use as an inhibitor against SARS-CoV-2 [18]. In another theoretical study, Halim and et al. investigated the ability of over fifty peptides

* Corresponding author.
E-mail address: izadyar@um.ac.ir (M. Izadyar).

https://doi.org/10.1016/j.molliq.2021.117852
0167-7322/

as antiviral agents for novel coronavirus [19]. Their obtained results indicated that peptides having greater affinity to Tyr489 and Tyr505 of RBD show a better inhibitory effect [19]. Moreover, peptides containing Tyr, Phe, Gly, Ala, Asn, Gln, and Cys have stronger interactions with the RBD of SARS-CoV-2.

In addition to finding a drug or antiviral agent for the SARS-CoV-2 designing selective and sensitive sensors for detection of the corresponding virus is of importance [20]. In this context, sensors based on nanostructures and biomaterials have considerable potential for selective detection of coronavirus [21]. For example, Ishikawa and coworkers designed a nanowire electrochemical sensor based on In_2O_3 for SARS-CoV-2 detection [22], which this sensor detects the N protein of coronavirus using an antibody mimic protein. Moreover, a fluorescent biosensor based on molybdenum disulfide (MoS_2) nanosheet was reported by Weng et al. to detect an avian coronavirus [23,24]. In this sensor, MoS_2 functionalized by an antibody can selectively detect the avian coronavirus. Broughton and coworkers designed a sensor based on the CRISPR-Cas12 gene for the detection of novel coronavirus. This sensor shows a greater sensitivity against SARS-CoV-2 in comparison with the FDA-approved RT-PCR test [25].

By employing theoretical methods [21,26], it is possible to design new sensors based on nanomaterial [27,28] including MoS_2 [29], graphene [30], and phosphorene nanosheets [31]. Previous studies indicated that molecular dynamics simulations can provide interesting results from the molecular viewpoint about the adsorption of the proteins on the phosphorene nanosheet. For example, Datta and coworkers investigated the adsorption of two dimeric proteins, namely the HIV-1 integrase and the λ_{6-85} repressor protein on black phosphorene nanosheet [32]. Their obtained results revealed that phosphorene nanosheets can make stable complexes with the corresponding proteins. Moreover, it is confirmed that the secondary structure of these proteins does not change after the adsorption on the surface of phosphorene.

In this article, by applying full atomistic molecular dynamics (MD) simulations, the interactions of RBD of SARS-CoV-2 with phosphorene nanosheet were investigated and compared with the RBD interactions with graphene. To design a sensitive and selective sensor for SARS-CoV-2 detection based on these nanosheets, molecular insight into the physiochemical process at the surface of the corresponding nanostructures is important.

In comparison to other 2D nanomaterials, it is possible to tune the band gap and properties of phosphorene nanosheet by changing the number of phosphorene layers by defects [33]. Moreover, phosphorene nanosheet has considerable mechanical flexibility, transparency, and high mechanical stability at ambient pressure [34–37]. Phosphorene nanosheets can be functionalized by various biomolecules [38], therefore the study of the interactions between RBD and phosphorene nanosheets can provide interesting results for designing sensors for the detection of SARS-CoV-2.

2. Theoretical methods

To study the dynamical behavior of RBD in the presence of graphene and phosphorene nanosheets, full atomistic molecular dynamics (MD) simulations were applied. The crystal structure of the RBD of the SARS-CoV-2 was obtained from the protein data bank (PDB) with the 6M17 code. The black phosphorene and graphene nanosheets were placed at the bottom of a cubic box ($10 \times 10 \times 10$ nm^3, Figure S1). RBD having different orientations (ORs) was placed parallel relative to the surface of the nanostructures with the minimum distance of 10 Å. In other words, RBD can interact with the surface of graphene or phosphorene nanosheet in six ways, therefore the dynamical behavior of the RBD was analyzed in the presence of these nanostructures through twelve independent MD simulations. Then each system was fully solvated by water molecules (TIP3P water model) [39,40]. To neutralize the charge of the RBD, Na^+, and Cl^- counter ions were added and the MD simulations were performed in the presence of 150 mM NaCl (physiological solution).

The reported parameters by Cheatham and coworkers were employed for Na^+ and Cl^- ions [41]. These parameters can reproduce the properties of NaCl solution and do not form any salt crystal or ion pair in water, which is an important factor for simulating the effects of physiological solution on biomolecules [42].

The MD simulation was started by 100,000 steps of energy minimization on the structures in water. Then the temperature of the systems increased from 0 to 298.15 K during 10 ns with 1 fs time step in an NVT ensemble by employing the typical force constant of 2.5 kcal.mol^{-1}.A^2 for solute structure. After this step, the corresponding systems were equilibrated during 20 ns with 1 fs time step in an NPT ensemble (298.15 and 1 bar) without any positional restraint. Finally, 200 ns NPT MD simulation (product step) was performed with 2 fs time step on the obtained structures from the equilibrated step. To investigate the dynamical behavior of the RDB another 200 ns MD simulation was performed in the absence of graphene and phosphorene nanosheets (see Figure S1, minimization, heating, and equilibration steps for this system are the same as conditions reported for RBD with nanostructures.).

The General Amber Force Field (GAFF) parameters [43,44] and FF14SB force field [45–48] were employed for the nanosheets and RBD, respectively. It is well worth mentioning that to simulate the structure of the phosphorene nanosheet, it is assumed that the force constants for all bond and angle types in the force field parameters are identical according to the prior studies [49,50].

The periodic boundary conditions were employed in all directions for the studied systems. In the NPT simulations, the Langevin thermostat and isotropic Berendsen method were applied to control the temperature and pressure with a collision frequency of 5 ps^{-1} and the relaxation time of 1 ps for temperature and pressure, respectively [51–56]. The Particle Mesh Ewald (PME) method with 10 Å direct cutoff was used to calculate the long-range electrostatic interactions [57]. The SHAKE constraints were applied for all bonds involving hydrogen atoms [58]. The Amber 14 software package was employed for doing all molecular dynamic simulations [59].

To calculate the binding energies by employing MD simulation for the RBD interactions with phosphorene and graphene surfaces, the molecular mechanics Generalized Born Surface Area (MM-GBSA) method was applied [60–64]. The entropy contribution was calculated by using harmonic approximation and the binding energies were calculated from the final 50 ns of the product step.

3. Results and discussion

3.1. Dynamics of RBD

The interaction between RBD of the SARS-CoV-2 and ACE2 receptor is the main step of virus entry to the cell. Therefore, RBD can be a target for drug development and sensor design for the coronavirus. In this context, 200 ns MD simulations were applied to investigate the dynamical behavior and structural properties of RBD in the physiological solution.

Fig. 1a shows the obtained structure of RBD after the simulation time. According to this figure, the structure of RBD is divided into core and contact regions (CR). The core region is composed of five antiparallel strand β-sheet with connected short α-helices and loops. In these β-sheets, there are 11 hydrogen bonds (H-bonds) between the residues, which play a key role in the stability of these strands. The contact regions (CRs) of the RBD with the ACE2 (Fig-

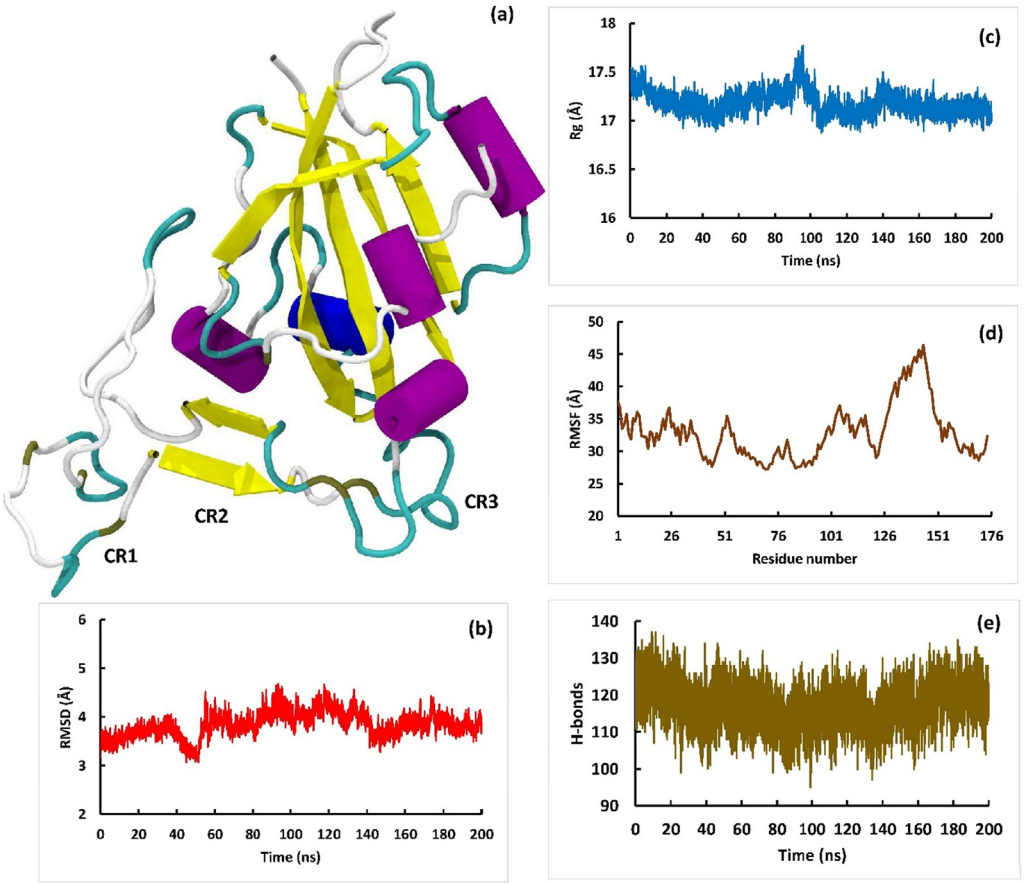

Fig. 1. The obtained structure of RBD after simulation time (a) and the calculated RMSD (b), Rg (c), RMSF (d), and number of H-bonds (e) of the RBD during 200 ns MD simulations.

ure S2) consist of loops (CR1), β-sheets (CRs), and helices (CR3). The CR2 which is in the middle of the RBD interaction with ACE2 composed of two short strands of β-sheets that these strands have been stabilized by two internal H-bonds.

To study the structural stability of the RBD during the simulation time, root mean square deviation (RMSD) values were calculated. According to Fig. 1b, the calculated RMSD values confirm that RBD has considerable stability in the physiological solution (RMSD = 3.84 ± 0.25 Å) and the system has reached equilibrium. To compare the obtained RBD structure from the MD simulation with the crystallography structure, the simulated RBD was aligned to the crystal structure (Figure S3). Based on the calculated RMSD value (3.33 Å) of the aligned structures, the simulated RBD has remarkable stability in water confirming our computational setting. Fig. 1c shows the calculated radii of gyration (Rg) values of RBD during 200 ns MD simulations. According to this figure, the calculated average value of Rg for the RBD is 17.18 ± 0.11 Å, confirming the structural stability because a larger Rg indicates that the structure is less compact and has greater fluctuations during the simulation.

Root mean square fluctuation (RMSF) analysis (Fig. 1d) can provide information about the dynamics of the residue concerning its initial position. On the basis of the structural analysis the CR1, CR2, and CR3 consist of residues 134–146, 147–154, and 155–164, respectively. According to the calculated RMSF values, the residues in the range of 120–150 have the maximum fluctuation in comparison with other residues, which confirms that CR1 and CR2 of the RBD have higher flexibility and fluctuation during the simulation time than the core region and CR3 of the RBD. Hydrogen bond interactions have a crucial role in the stability of proteins. For the hydrogen bond analysis, the existence of a hydrogen bond was determined based on a cut-off distance of 3.5 Å between the acceptor and the donor atoms of the hydrogen bond as well as a cut-off of 30° for the hydrogen-donor–acceptor angle. The calculated average number of H-bonds of RBD indicated that this protein has 117.20 ± 5.69 internal H-bonds. Moreover, the comparison between the trend of the calculated number of H-bonds (Fig. 1e) and RMSD values during the simulation time confirms that increasing the internal H-bonds elevate the RBD stability.

3.2. Dynamics of RBD on the surface of graphene and phosphorene nanosheets

As mentioned before, the RBD interaction with the ACE2 receptor is the main step of virus entry to the cell. Therefore, the study of the RBD interaction with graphene and phosphorene nanosheets can provide useful results for designing new sensors based on these nanostructures for SARS-CoV-2 detection. To investigate the RBD interactions with phosphorene and graphene nanosheets, its dynamical behavior was analyzed by considering different initial orientations relative to the corresponding nanostructures.

Fig. 2 shows the obtained structures of RBD after the simulation time in the presence of the graphene nanosheet. In this figure, OR1 shows the RBD interaction with graphene surface from the contact region side (CR1, CR2, and CR3). In contrast, the second orientation (OR2) shows an opposite orientation for the RBD interaction relative to the surface when the binding site is on the top. Overall, RBD can interact with the surface through six paths, in which

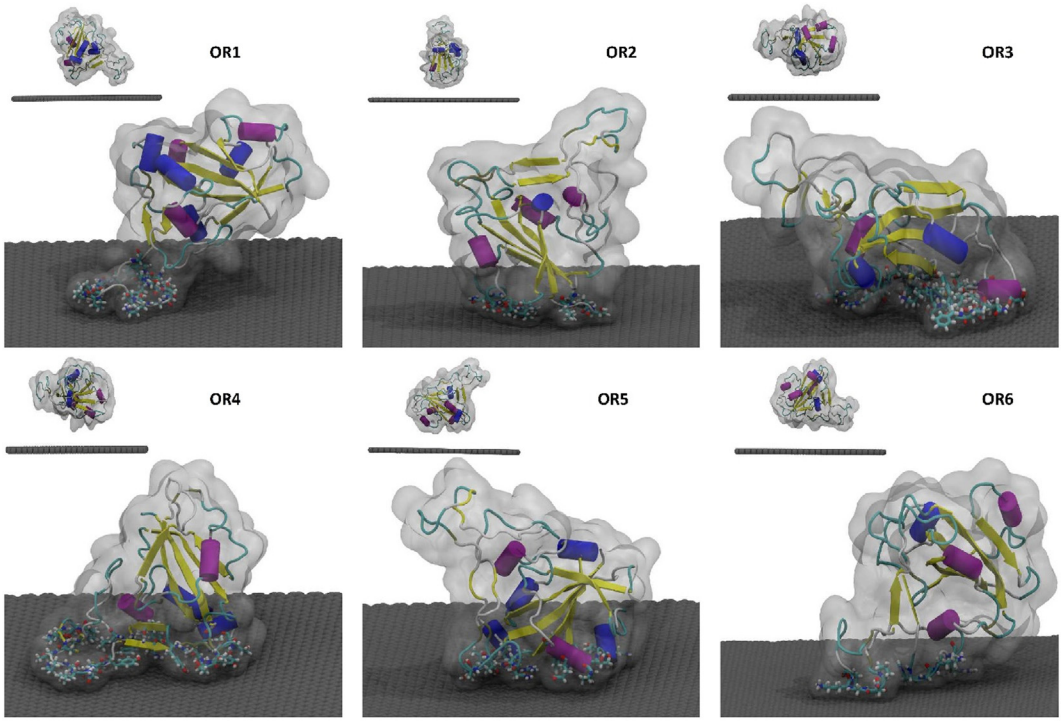

Fig. 2. The obtained structures of the RBD, having different initial orientations, in the presence of graphene nanosheet after the simulation time. The initial configurations are represented as the small figures on the top corner.

OR1, OR3, and OR5 are in opposite directions relative to the surface in comparison with OR2, OR4, and OR6, respectively.

According to Fig. 2, the obtained structure of OR1 shows that, after the simulation time, the RBD interacts with the graphene surface through the CR1, while at the initial step of the simulation, CR1, CR2, and CR3 have an equal distance approximately relative to the surface. Moreover, structural analysis indicates that RBD maintains its secondary structure in the presence of graphene. In other words, the interaction of graphene and RBD has no important effect on the secondary structure and folding properties of the RBD. According to Fig. 2, RBD spreads on the graphene surface through OR3 and OR4. These interactions are more important in comparison with other orientations from the energy point of view. Based on the obtained results, the contact regions (CR1, CR2, and CR3) of the RBD have the maximum interactions with the graphene surface. According to Fig. 2, the initial configurations are different, but the RBD-graphene complexes, after the simulation time, indicate that RBD prefers to interact with graphene from the contact region (except OR2).

Fig. 3 shows the structure of RBD after the simulation time on the surface of the phosphorene nanosheet. According to this figure, the dynamical behavior of the RBD on the surface of phosphorene is different in comparison with the graphene surface. According to Fig. 3, all CRs of the RBD interact with the phosphorene nanosheet in OR1, which is in contrast to graphene. In the presence of graphene, only CR1 of the RBD interacts with the surface. Moreover, no residue of the binding site interacts with the phosphorene surface in the cases of OR3 and OR4, which is in contrast to the RBD-graphene complex.

To investigate the structural stability of RBD on the surface of graphene and phosphorene, RMSD analysis was applied (Figure S4). According to Fig. 4a, RBD has a lower structural fluctuation in the absence of nanostructures. This means that the RBD interaction with the surfaces negligibly reduces its stability. The comparison between the calculated RMSD values in the presence of graphene and phosphorene reveals that RBD has greater stability on the phosphorene surface than that of graphene. The calculated Rg values of the RDB (Fig. 4b) confirm that RBD spreads on the surface of these nanostructures and RBD has lower compaction in the presence of graphene and phosphorene (OR1, OR3, OR4, and OR6).

Internal H-bond interaction is one of the important factors in the structural stability of proteins. Fig. 4c shows the calculated average number of H-bonds of RBD in the presence and absence of graphene and phosphorene nanosheets. According to this figure, RBD has the maximum of internal H-bond interactions on the graphene and phosphorene surfaces through OR4 and OR3, respectively. The remarkable point is that there is a direct relationship between Rg and the number of H-bonds. For example, the maximum Rg value is obtained when RBD interacts with graphene through OR3. On the other hand, due to lower structural compaction, the possibility of internal H-bond interactions decreases, which is in agreement with the calculated number of hydrogen bonds.

RBD has a greater solvent accessible surface area (SASA) in the presence of the nanostructures because RBD spreads on the surface of graphene and phosphorene due to complex formation (Fig. 4d). Moreover, the calculated SASA values confirm the obtained results of the Rg and H-bond analyses.

The calculated RMSF values indicate that the residues of the RBD have lower flexibility of the phosphorene surface in comparison with graphene (Fig. 5). According to Fig. 5a, RBD has the maximum and minimum stability through OR6 and OR4, respectively, due to the interactions with graphene. In contrast to graphene, RBD represents remarkable stability on the phosphorene surface (Fig. 5b), according to the calculated RMSF values. Based on Fig. 5b, the calculated maximum RMSF value of RBD in the presence of phosphorene is 12.04 Å, which confirms a considerable interaction of RBD and phosphorene.

On the basis of obtained results, the dynamical behavior of RBD is different on the phosphorene and graphene surfaces. This means that RBD has greater stability or lower fluctuation in the presence of phosphorene in comparison with graphene. Therefore, it can be

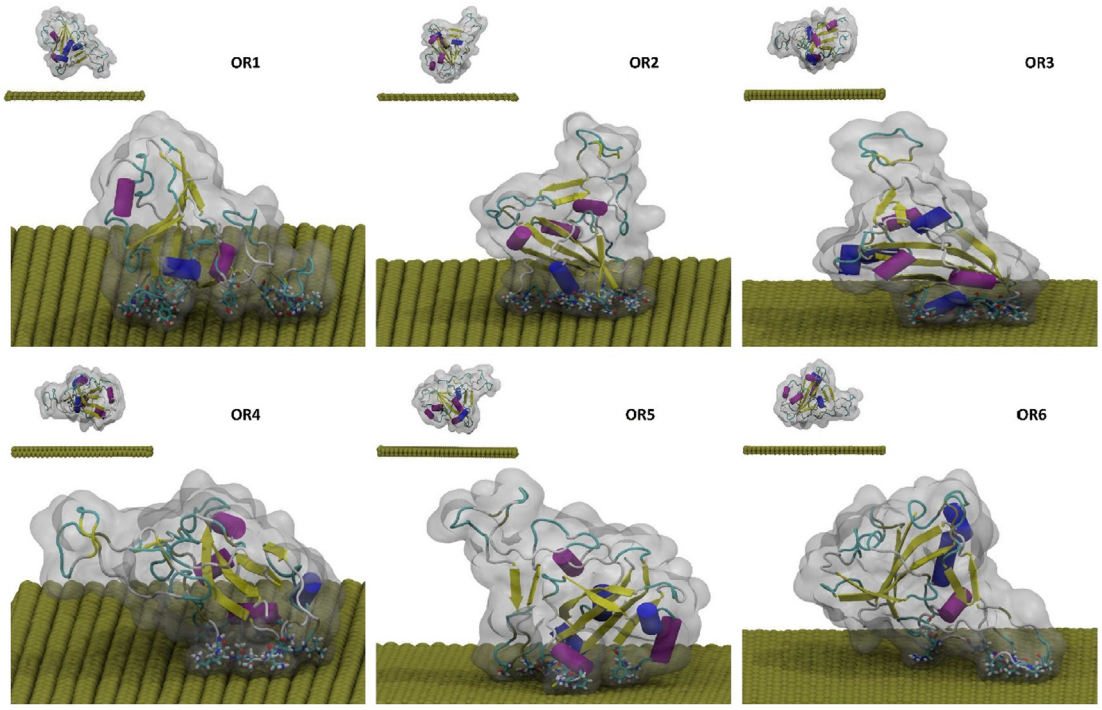

Fig. 3. The obtained structures of the RBD complexes with phosphorene nanosheet after the simulation time with different initial orientations relative to the surface. The initial configurations are represented as the small figures on the top corner.

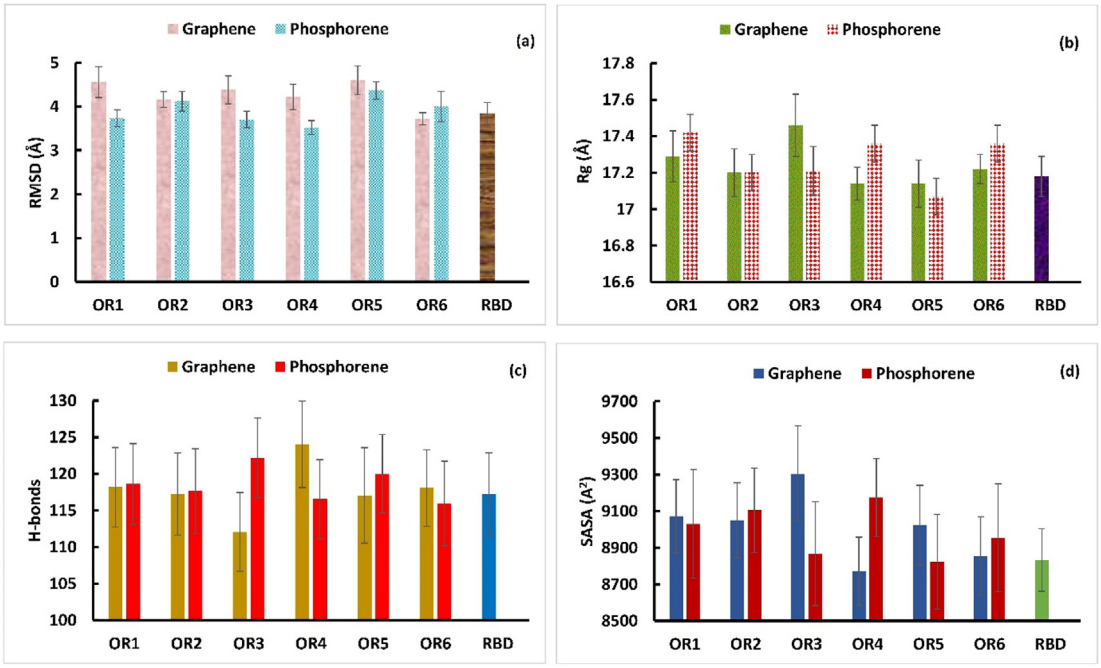

Fig. 4. The calculated average values of RMSD (a), Rg (b), the number of the internal H-bonds (c), and SASA (d) of the RBD in the presence and absence of the nanostructures.

claimed that phosphorene can form a more stable complex with RBD than graphene.

3.3. RBD interactions with phosphorene and graphene nanosheets

To have an insight into the sensitivity of graphene and phosphorene nanosheets against RBD, the possible interactions in the complexes were analyzed. Fig. 6a shows the calculated average number of the contacts between RBD and surfaces of the nanostructures (with 4 Å cutoff). According to this figure, the amino acid residues of the RBD have greater interactions with phosphorene in comparison with graphene. Moreover, based on the calculated number of contacts, RBD has maximum contact with graphene and phosphorene surfaces through OR5 and OR6, respectively. On the other hand, the calculated average center of mass distance between the RBD and the nanostructures confirms that RBD prefers

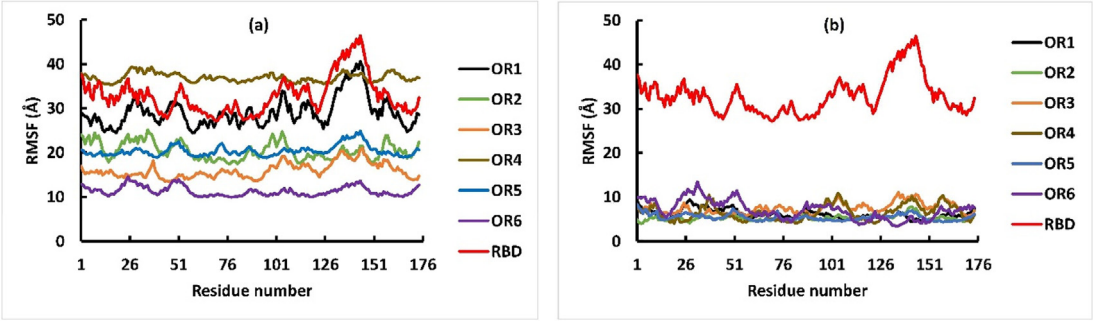

Fig. 5. The calculated RMSF values for the RBD in the presence of graphene (a) and phosphorene nanosheets (b).

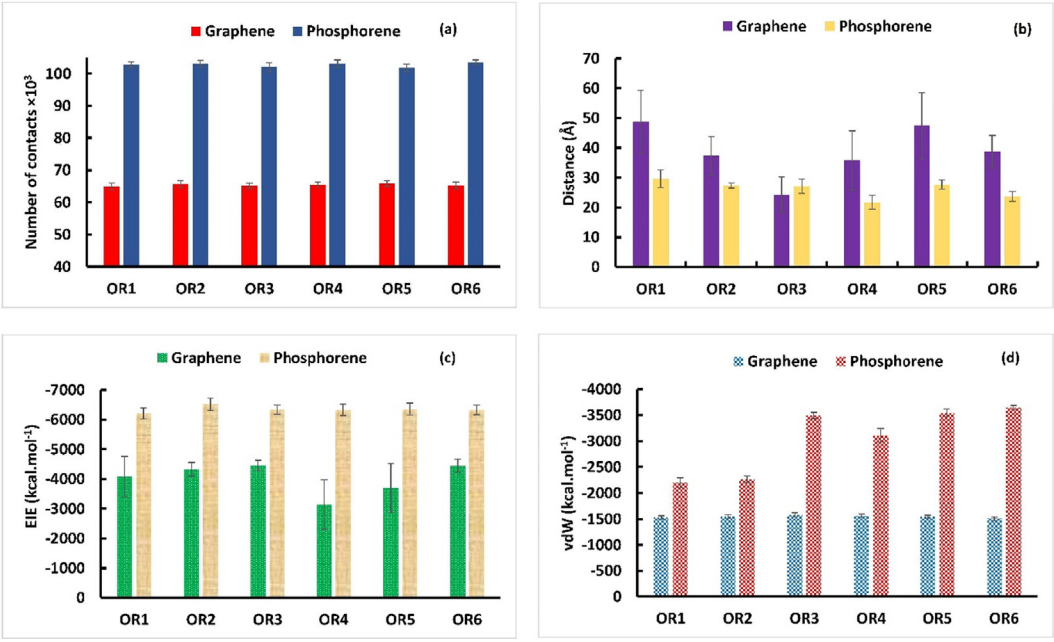

Fig. 6. The calculated average number of contacts (a), center of mass distance (b) EIE (c), and vdW interaction energy between RBD and graphene and phosphorene surfaces.

to interact with phosphorene than graphene (Fig. 6b). According to Fig. 6b, RBD has the maximum interaction with graphene surface through OR3. Because through this orientation, this protein lies in the closest distance relative to the graphene surface, which is in agreement with the previous results (Rg and H-bond analyses).

In the presence of phosphorene nanosheet, the distances of the RBD relative to the surface are in the range of 2.2–2.9 nm. OR4 has the minimum distance with the phosphorene surface in comparison with other orientations. Phosphorene and graphene can adsorb RBD due to electrostatic and van der Waals (vdW) interactions. Therefore, the electrostatic and vdW interactions between RBD and different nanostructures were calculated by employing the linear interaction energy (LIE) analysis method [65]. According to the calculated values of the electrostatic interaction energy (EIE) and vdW interaction energy (Fig. 6), the electrostatic interactions between RBD and the surface of the nanostructures have a greater effect on the stability of nanostructure-RBD complexes in comparison with vdW interactions. Fig. 6-c shows that RBD can form more stable complexes with phosphorene than graphene due to greater electrostatic interactions. In other words, phosphorene represents a higher sensitivity against RBD in comparison with graphene.

The comparison between the calculated EIE values reveals that RBD has the highest electrostatic interaction with graphene through OR3, while this protein forms the most stable complex with phosphorene through OR2. The calculated vdW interaction energies (Fig. 6d) are similar to the mentioned analyses confirming that phosphorene nanosheet has a greater affinity to RBD than graphene. Moreover, the vdW interactions of the RBD-graphene and RBD-phosphorene are greater through OR3 and OR6, respectively.

Trajectory analysis indicates that the dynamics and behavior of RBD are different on the surface of phosphorene and graphene nanosheet. To study the effect of the RBD interaction with these nanostructures on the dynamical behavior, free energy landscape (FEL) analysis was applied [66]. The FEL analysis provides interesting details on the RBD interactions by identifying the structural changes of this protein [66]. Moreover, this method correlates the structure to the dynamical behavior and stability of biomolecules.

Fig. 7 shows the FEL of the RBD in the presence and absence of phosphorene. The minimum point of the FEL identifies the most stable conformation of the RBD during the simulation time. The FEL of the RBD changes in the presence of the nanostructures, which confirms that RBD has considerable interactions with the surfaces of graphene and phosphorene. The difference in the shape of the FELs of RBD in the presence of phosphorene (Fig. 7) and graphene (Figure S5) reveals that the strength of the RBD interactions with these surfaces is different having unique dynamics on the surface of each nanostructure.

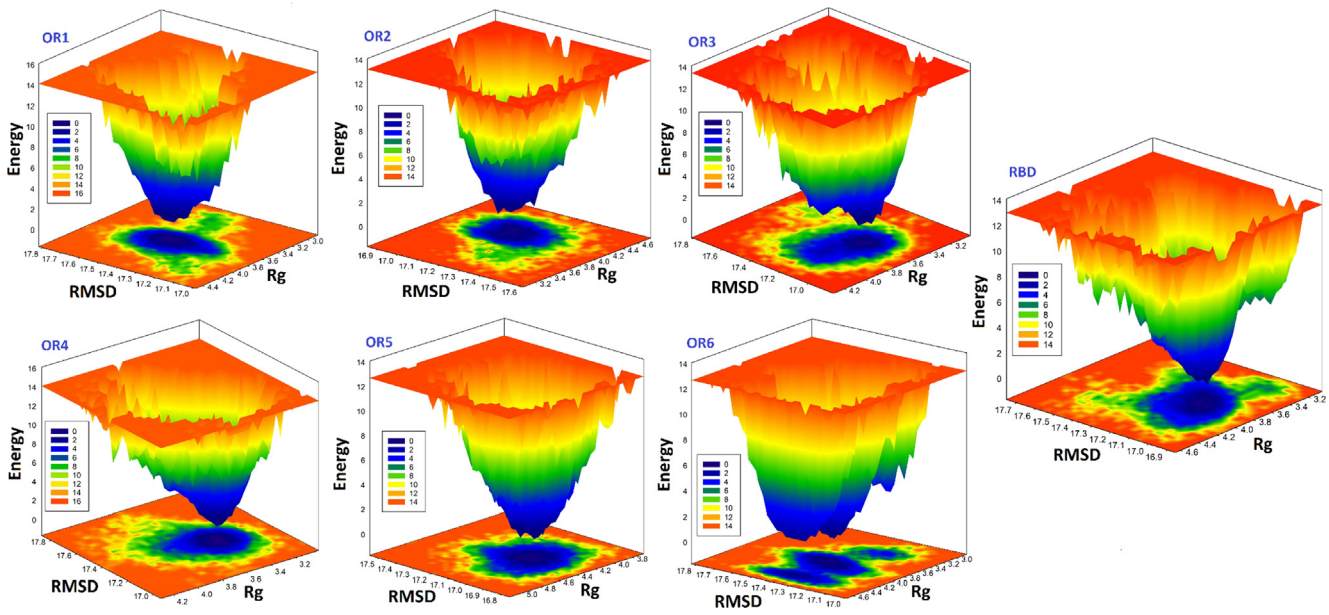

Fig. 7. The calculated FEL of the RBD in the presence and absence of phosphorene. The RMSD, Rg, and energy are in Å and kcal mol^{-1}, respectively.

Overall, based on the calculated values of EIE and vdW interactions, the role of the electrostatic interactions is more important on the stability of RBD complexes with different surfaces. Moreover, it can be concluded that RBD forms the most stable complexes with phosphorene and graphene in the OR2 and OR3, respectively. Moreover, the phosphorene nanosheet shows higher sensitivity against this protein in comparison with graphene. Based on the FEL analysis, the interaction between the RBD and surfaces changes the dynamical behavior and structural stability of the RBD.

3.4. Binding energy

To have a quantitative insight into the stability of the RBD complexes with phosphorene and graphene nanosheets, Gibbs binding energies were calculated by employing the MM-GBSA method. According to the calculated Gibbs binding energy in the gas phase (ΔG_{gas}), the complex formation between RBD and different nanostructures is favorable from the thermodynamic viewpoint (Table 1). Moreover, RBD forms more stable complexes with graphene than phosphorene in the gas phase except through OR2. Actually, through this orientation, the most stable complex is obtained in the presence of the phosphorene nanosheet. On the basis of the calculated Gibbs binding energy in the solution phase (ΔG_{sol}), in contrast to the gas phase, the complexation process is not favorable thermodynamically ($\Delta G_{sol} > 0$). In other words, solvent reduces the stability of the RBD complexes with the corresponding nanostructures. This result indicates the remarkable role of the solvent on the interaction between RBD and the surfaces. The calculated total Gibbs binding energy (ΔG_{tot}) confirms that the orientation of the RBD relative to the graphene and phosphorene is important, which changes the stability of the corresponding complexes. Moreover, through OR3 and OR6, RBD forms more stable complexes with graphene in comparison with the phosphorene. RBD forms the most stable complexes with graphene and phosphorene through OR3 and OR2, confirmed by the calculated ΔG_{tot} values (-83.65 and −200.37 kcal.mol^{-1}, respectively). Therefore, it can be concluded that phosphorene has more affinity and sensitivity against RBD in comparison with graphene.

Electrostatic and vdW interactions have key roles in the stability of the RBD complexes with the nanostructures. Moreover, these parameters are the main part of the calculated Gibbs binding energy. MM-GBSA and LIE methods confirm that RBD has lower vdW and electrostatic interactions with graphene than phosphorene. Therefore, the calculated values of ΔG_{tot} for the graphene-RBD complexes show less stability in comparison with the phosphorene-RBD complexes.

There is an interesting trend between the calculated EIE by linear interaction energy (LIE) analysis and the calculated ΔG_{tot} by

Table 1
The calculated Gibbs binding energies (kcal.mol^{-1}) of the RBD complexes with graphene and phosphorene nanosheets.

Graphene	ΔG_{gas}	SD	ΔG_{sol}	SD	ΔG_{tot}	SD
OR1	−166.47	6.45	90.68	4.23	−75.79	4.24
OR2	−122.30	5.01	59.55	2.88	−62.74	3.87
OR3	−170.80	7.64	87.15	5.40	−83.65	5.65
OR4	−167.82	6.49	101.07	6.24	−66.74	3.80
OR5	−153.40	10.52	100.30	7.45	−53.10	5.72
OR6	−143.85	12.57	88.50	9.40	−55.35	6.06
Phosphorene						
OR1	−149.67	4.48	45.23	2.95	−104.43	3.29
OR2	−293.11	6.24	92.73	3.74	−200.37	5.53
OR3	−100.91	6.13	25.68	3.34	−75.23	3.79
OR4	−103.73	7.11	35.14	4.07	−68.58	4.62
OR5	−98.12	13.91	28.41	4.76	−69.71	11.17
OR6	−104.54	3.49	54.10	2.80	−50.44	2.49

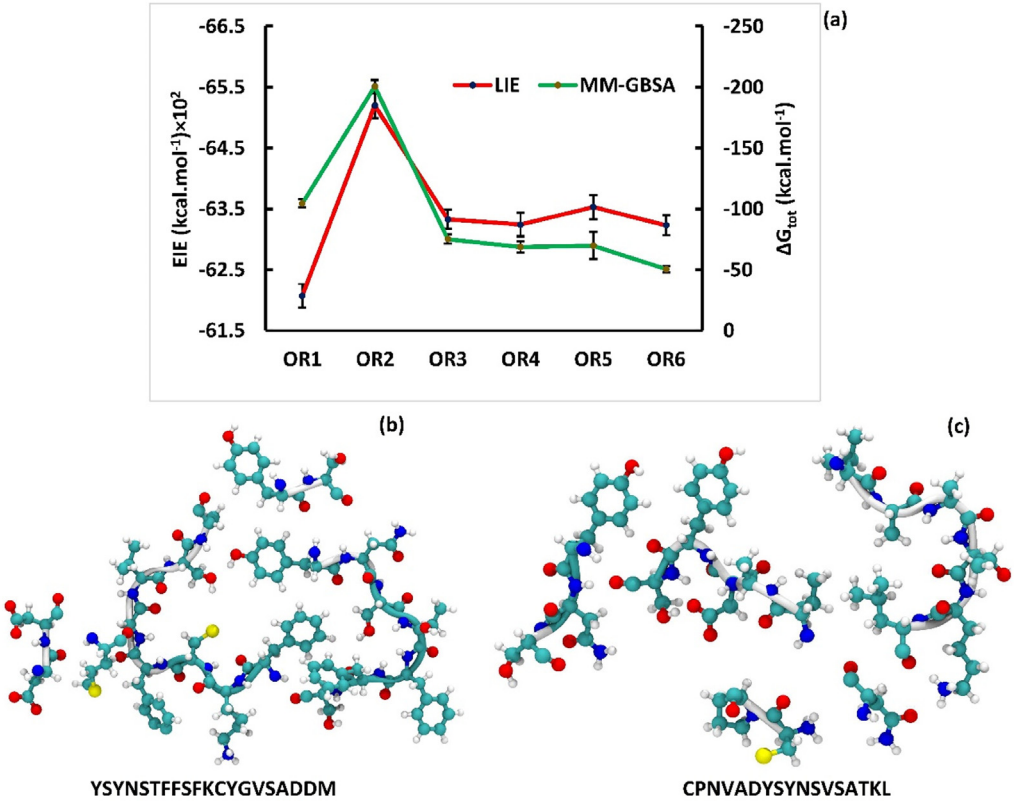

Fig. 8. The predicted trend between the calculated electrostatic interactions with the LIE method and the total binding Gibbs energy of the RBD complex with phosphorene nanosheet (a) and the amino acid residues involved in the RBD interactions with graphene (b) and phosphorene (c).

MM-GBSA method for the RBD interaction with phosphorene surface. According to Fig. 8a, both LIE and MM-GBSA methods predict that RBD has the most stable complex with the phosphorene nanosheet through OR2. This result confirms that electrostatic interactions between RBD and the surface of the nanostructure have key roles in the stability of the corresponding complexes because the trend of the electrostatic interactions and the calculated total Gibbs binding energy is the same. The interaction strength and dynamical behavior of RBD in the presence of phosphorene and graphene are different because the involved amino acid residues are different, according to Fig. 8b and c. The calculated interaction energies for RBD interactions with phosphorene nanosheet indicate that the electrostatic interaction has a greater contribution than vdW interaction in the stability of the RDB-phosphorene complex. This result is due to the polar and charged nature of the involved residues in the interactions between phosphorene nanosheet and RBD (Fig. 8c).

4. Conclusion

Molecular dynamics simulation was applied to investigate the affinity of graphene and phosphorene nanosheets against RBD of the SARS-CoV-2. On the basis of the obtained results, these nanostructures change the structural stability of the RBD. This protein has lower structural stability with graphene in comparison with the phosphorene nanosheet. The FEL analysis reveals that RBD has considerable interactions with the surfaces of graphene and phosphorene nanosheet. Moreover, graphene and phosphorene nanosheets can change the dynamical behavior of this protein due to strong interactions with RBD. The electrostatic and vdW interactions between RBD and the surfaces of graphene and phosphorene have a key role in the stability of RBD complexes with the corresponding nanostructures. The strength of the RBD interactions with phosphorene and graphene and their dynamical behavior on their surfaces are different because of the variety of the involved amino acid residues in the corresponding interaction sites. RBD forms a more stable complex with phosphorene due to greater electrostatic and vdW interactions in compassion with graphene. Moreover, based on the calculated binding energies, phosphorene nanosheet shows greater sensitivity and affinity against RBD than graphene. Finally, based on different analyses, phosphorene has a considerable ability for using as an agent for designing new sensors to detect SARS-CoV-2.

Declaration of Competing Interest

The authors declare that they have no known competing financial interests or personal relationships that could have appeared to influence the work reported in this paper.

Acknowledgement

Aliyeh Mehranfar was partially supported by a grant from Ferdowsi University of Mashhad (No. FUM-41073). We hereby acknowledge that part of this computation was performed at the Sci-HPC center of Ferdowsi University of Mashhad.

Appendix A. Supplementary material

Supplementary data to this article can be found online at https://doi.org/10.1016/j.molliq.2021.117852.

References

[1] R. Yan, Y. Zhang, Y. Li, L. Xia, Y. Guo, Q. Zhou, Structural basis for the recognition of SARS-CoV-2 by full-length human ACE2, Science 367 (2020) 1444–1448.

[2] N. Chen, M. Zhou, X. Dong, J. Qu, F. Gong, Y. Han, Y. Qiu, J. Wang, Y. Liu, Y. Wei, Epidemiological and clinical characteristics of 99 cases of 2019 novel coronavirus pneumonia in Wuhan, China: a descriptive study, The Lancet 395 (2020) 507–513.

[3] P. Zhou, X.-L. Yang, X.-G. Wang, B. Hu, L. Zhang, W. Zhang, H.-R. Si, Y. Zhu, B. Li, C.-L. Huang, A pneumonia outbreak associated with a new coronavirus of probable bat origin, Nature 579 (2020) 270–273.

[4] M. Mehranfar, Izadyar, Theoretical Design of Functionalized Gold Nanoparticles as Antiviral Agents against Severe Acute Respiratory Syndrome Coronavirus 2 (SARS-CoV-2), J. Phys. Chem. Lett. 11 (2020) 10284–10289.

[5] Z. Xu, L. Shi, Y. Wang, J. Zhang, L. Huang, C. Zhang, S. Liu, P. Zhao, H. Liu, L. Zhu, Pathological findings of COVID-19 associated with acute respiratory distress syndrome, Lancet Respir. Med. 8 (2020) 420–422.

[6] F. Wu, A. Wang, M. Liu, Clinical features of patients infected with 2019, novel coronavirus in Wuhan, China, Lancet 395 (2020) 497–506.

[7] D. Paraskevis, E.G. Kostaki, G. Magiorkinis, G. Panayiotakopoulos, G. Sourvinos, S. Tsiodras, Full-genome evolutionary analysis of the novel coronavirus (2019-nCoV) rejects the hypothesis of emergence as a result of a recent recombination event, Infect. Genet. Evol. 79 (2020) 104212.

[8] F. Li, Structure, function, and evolution of coronavirus spike proteins, Annu. Rev. Virol 3 (2016) 237–261.

[9] Q. Wang, Y. Zhang, L. Wu, S. Niu, C. Song, Z. Zhang, G. Lu, C. Qiao, Y. Hu, K.-Y. Yuen, Structural and functional basis of SARS-CoV-2 entry by using human ACE2, Cell 181 (2020), 894–904. e899.

[10] M. Ghorbani, B.R. Brooks, J.B. Klauda, Critical sequence hotspots for binding of novel coronavirus to angiotensin converter enzyme as evaluated by molecular simulations, J. Phys. Chem. B 124 (2020) 10034–10047.

[11] B.J. Bosch, R. Van der Zee, C.A. De Haan, P.J. Rottier, The coronavirus spike protein is a class I virus fusion protein: structural and functional characterization of the fusion core complex, J. Virol. 77 (2003) 8801–8811.

[12] Y. Wan, J. Shang, R. Graham, R.S. Baric, F. Li, Receptor recognition by the novel coronavirus from Wuhan: an analysis based on decade-long structural studies of SARS coronavirus, J. Virol. 94 (2020) e00127–00120.

[13] D. Wrapp, N. Wang, K.S. Corbett, J.A. Goldsmith, C.-L. Hsieh, O. Abiona, B.S. Graham, J.S. McLellan, Cryo-EM structure of the 2019-nCoV spike in the prefusion conformation, Science 367 (2020) 1260–1263.

[14] L. Zhou, Y. Liu, W. Zhang, P. Wei, C. Huang, J. Pei, Y. Yuan, L. Lai, Isatin compounds as noncovalent SARS coronavirus 3C-like protease inhibitors, J. Med. Chem. 49 (2006) 3440–3443.

[15] Y. Han, P. Král, Computational design of ACE2-based peptide inhibitors of SARS-CoV-2, ACS nano 14 (2020) 5143–5147.

[16] J. Xu, P.-Y. Shi, H. Li, J. Zhou, Broad spectrum antiviral agent niclosamide and its therapeutic potential, ACS Infect. Dis. 6 (2020) 909–915.

[17] B. Nutho, P. Mahalapbutr, K. Hengphasatporn, N.C. Pattaranggoon, N. Simanon, Y. Shigeta, S. Hannongbua, T. Rungrotmongkol, Why are lopinavir and ritonavir effective against the newly emerged coronavirus 2019? Atomistic insights into the inhibitory mechanisms, Biochemistry 59 (2020) 1769–1779.

[18] J. Wang, Fast identification of possible drug treatment of coronavirus disease-19 (COVID-19) through computational drug repurposing study, J. Chem. Inf. Model 60 (2020) 3277–3286.

[19] S.M. Chowdhury, S.A. Talukder, A.M. Khan, N. Afrin, M.A. Ali, R. Islam, R. Parves, A. Al Mamun, M.A. Sufian, M.N. Hossain, Antiviral peptides as promising therapeutics against SARS-CoV-2, J. Phys. Chem. B 124 (2020) 9785–9792.

[20] S.P. Varahachalam, B. Lahooti, M. Chamaneh, S. Bagchi, T. Chhibber, K. Morris, J. F. Bolanos, N.-Y. Kim, A. Kaushik, Nanomedicine for the SARS-CoV-2: state-of-the-art and future prospects, Int. J. Nanomed. 16 (2021) 539.

[21] M. Khavani, M. Izadyar, S. Samadian, QM/MD study on the ability of phosphorene for selective detection of amino acids, J. Mol. Liq. 336 (2021) 116865.

[22] F.N. Ishikawa, H.-K. Chang, M. Curreli, H.-I. Liao, C.A. Olson, P.-C. Chen, R. Zhang, R.W. Roberts, R. Sun, R.J. Cote, Label-free, electrical detection of the SARS virus N-protein with nanowire biosensors utilizing antibody mimics as capture probes, ACS nano 3 (2009) 1219–1224.

[23] X. Weng, S. Neethirajan, Immunosensor based on antibody-functionalized MoS 2 for rapid detection of avian coronavirus on cotton thread, IEEE Sensors J. 18 (2018) 4358–4363.

[24] P. Teengam, W. Siangproh, A. Tuantranont, T. Vilaivan, O. Chailapakul, C.S. Henry, Multiplex paper-based colorimetric DNA sensor using pyrrolidinyl peptide nucleic acid-induced AgNPs aggregation for detecting MERS-CoV, MTB, and HPV oligonucleotides, Anal. Chem. 89 (2017) 5428–5435.

[25] J.P. Broughton, X. Deng, G. Yu, C.L. Fasching, V. Servellita, J. Singh, X. Miao, J.A. Streithorst, A. Granados, A. Sotomayor-Gonzalez, CRISPR–Cas12-based detection of SARS-CoV-2, Nat. Biotechnol. 38 (2020) 870–874.

[26] M. Khavani, M. Izadyar, A comprehensive study of the solvent effects on the cycloaddition reaction of diethyl azodicarboxylate and ethyl vinyl ether: Efficient implementation of QM and TD-DFT study, Int. J. Quantum Chem. 115 (2015) 381–388.

[27] M. Khavani, M. Izadyar, M.R. Housaindokht, DFT study on the selective complexation of B12N12 nanocage with alkali metal ions, Phosphorus, Sulfur, and Silicon and the Related Elements, 193 (2018) 178–184.

[28] P. Snehha, V. Nagarajan, R. Chandiramouli, Interaction behavior of cyanogen fluoride and chloride gas molecules on red phosphorene nanosheet: a DFT study, J. Inorg. Organomet. Polym. Mat. 29 (2019) 954–963.

[29] C. Jian, W. Hong, Q. Cai, J. Li, W. Liu, Surface electron state engineering enhanced hydrogen evolution of hierarchical molybdenum disulfide in acidic and alkaline media, Appl. Catal. B 266 (2020) 118649.

[30] X. Gao, Q. Zhou, J. Wang, L. Xu, W. Zeng, Performance of intrinsic and modified graphene for the adsorption of H2S and CH4: A DFT study, Nanomaterials 10 (2020) 299.

[31] N.P. Shetti, S.J. Malode, D.S. Nayak, S.D. Bukkitgar, G.B. Bagihalli, R.M. Kulkarni, K.R. Reddy, Novel nanoclay-based electrochemical sensor for highly efficient electrochemical sensing nimesulide, J. Phys. Chem. Solids 137 (2020) 109210.

[32] T.K. Mukhopadhyay, A. Ghosh, A. Datta, Molecular dynamics simulations reveal orientation-dependent nanotoxicity of black phosphorene toward dimeric proteins, ACS Appl. Nano Mater. 4 (2021) 3095–3107.

[33] X. Peng, A. Copple, Q. Wei, Edge effects on the electronic properties of phosphorene nanoribbons, J. Appl. Phys. 116 (2014) 144301.

[34] L. Mao, H. Jin, M. Wang, Y. Hu, S. Chen, Q. He, J. Chang, C. Hong, Y. Zhou, D. Wang, Neurologic manifestations of hospitalized patients with coronavirus disease 2019 in Wuhan China, JAMA Neurol. 77 (2020) 683–690.

[35] D. John, R. Chatanathodi, Hydrogen adsorption on alkali metal decorated blue phosphorene nanosheets, Appl. Surf. Sci. 465 (2019) 440–449.

[36] D. John, B. Nharangatt, S.M. Kastuar, R. Chatanathodi, Blue phosphorene nanosheets with point defects: Electronic structure and hydrogen storage capability, Appl. Surf. Sci. 551 (2021) 149363.

[37] M.M.K. Dad, R. Pilevar, S. Ebrahimi, Ab-initio study of nanoporous phosphorene as anode material in rechargeable Li/Na ion batteries, Appl. Surf. Sci. (2021) 150155.

[38] P. Rubio-Pereda, G.H. Cocoletzi, Density functional theory calculations of biomolecules adsorption on phosphorene for biomedical applications, Appl. Surf. Sci. 427 (2018) 1227–1234.

[39] W.L. Jorgensen, J. Chandrasekhar, J.D. Madura, R.W. Impey, M.L. Klein, Comparison of simple potential functions for simulating liquid water, J. Chem. Phys. 79 (1983) 926–935.

[40] M. Khavani, M. Izadyar, M.R. Housaindokht, Modeling of the functionalized gold nanoparticle aggregation in the presence of dopamine: a joint MD/QM study, J. Phys. Chem. C 122 (2018) 26130–26141.

[41] I.S. Joung, T.E. Cheatham III, Determination of alkali and halide monovalent ion parameters for use in explicitly solvated biomolecular simulations, J. Phys. Chem. B 112 (2008) 9020–9041.

[42] Noy, I. Soteras, F.J. Luque, M. Orozco, The impact of monovalent ion force field model in nucleic acids simulations, Phys. Chem. Chem. Phys. 11 (2009) 10596–10607.

[43] J. Wang, R.M. Wolf, J.W. Caldwell, P.A. Kollman, D.A. Case, Development and testing of a general amber force field, J. Compu. Chem. 25 (2004) 1157–1174.

[44] M. Izadyar, M. Khavani, M.R. Housaindokht, Sensing ability of hybrid cyclic nanopeptides based on thiourea cryptands for different ions, A Joint DFT-D3/MD Study, J. Phys. Chem. A 121 (2017) 244–255.

[45] J.A. Maier, C. Martinez, K. Kasavajhala, L. Wickstrom, K.E. Hauser, C. Simmerling, ff14SB: improving the accuracy of protein side chain and backbone parameters from ff99SB, J. Chem. Theory Comput. 11 (2015) 3696–3713.

[46] M. Khavani, M. Izadyar, M.R. Housaindokht, RNA aptasensor based on gold nanoparticles for selective detection of neomycin B, molecular approach, J. Iran. Chem. Soc. 16 (2019) 2389–2400.

[47] M. Khavani, M. Izadyar, M.R. Housaindokht, Theoretical design and experimental study on the gold nanoparticles based colorimetric aptasensors for detection of neomycin B, Sens. Actuators B Chem. 300 (2019) 126947.

[48] M. Khavani, M. Izadyar, M.R. Housaindokht, The effects of amino acid sequence and solvent polarity on the self-assembling of cyclic peptide nanotubes and molecular channel formation inside the lipid bilayer, J. Mol. Liq. 314 (2020) 113660.

[49] V. Sresht, A.A. Padua, D. Blankschtein, Liquid-phase exfoliation of phosphorene: design rules from molecular dynamics simulations, ACS nano 9 (2015) 8255–8268.

[50] T.K. Mukhopadhyay, A. Datta, Ordering and dynamics for the formation of two-dimensional molecular crystals on black phosphorene, J. Phys. Chem. C 121 (2017) 10210–10223.

[51] D.J. Sindhikara, S. Kim, A.F. Voter, A.E. Roitberg, Bad seeds sprout perilous dynamics: stochastic thermostat induced trajectory synchronization in biomolecules, J. Chem. Theory Comput. 5 (2009) 1624–1631.

[52] B.P. Uberuaga, M. Anghel, A.F. Voter, Synchronization of trajectories in canonical molecular-dynamics simulations: observation, explanation, and exploitation, J. Chem. Phys. 120 (2004) 6363–6374.

[53] M. Khavani, R. Kalantarinezhad, M. Izadyar, A joint QM/MD study on α-, β-and γ-cyclodextrins in selective complexation with cathinone, Supramolecular Chem. 30 (2018) 687–696.

[54] M. Khavani, M. Izadyar, M.R. Housaindokht, A combined MD/QM study on the sensing mechanism of Pb2+ by glutathione functionalized gold nanoparticles, J. Mol. Liq. 280 (2019) 120–127.

[55] M. Khavani, M. Izadyar, M.R. Housaindokht, A molecular approach on the ability of functionalized gold nanoparticles for selective sensing of Hg2+, J. Mol. Liq. 292 (2019) 111461.

[56] M. Khavani, M. Izadyar, M.R. Housaindokht, MD/QM modeling of the modified gold nanoparticles and investigation of their sensing ability for selective detection of melamine, J. Mol. Liq. 284 (2019) 454–461.

[57] D.J. Tobias, K. Tu, M.L. Klein, Atomic-scale molecular dynamics simulations of lipid membranes, Curr. Opin. 2 (1997) 15–26.
[58] J.-P. Ryckaert, G. Ciccotti, H.J. Berendsen, Numerical integration of the cartesian equations of motion of a system with constraints: molecular dynamics of n-alkanes, J. Compu. Phys. 23 (1977) 327–341.
[59] D.A. Case, V. Babin, J. Berryman, R. Betz, Q. Cai, D. Cerutti, T. Cheatham Iii, T. Darden, R. Duke, H. Gohlke, Amber 14 (2014).
[60] B.R. Miller III, T.D. McGee Jr, J.M. Swails, N. Homeyer, H. Gohlke, A.E. Roitberg, MMPBSA. py: an efficient program for end-state free energy calculations, J. Chem. Theory Comput. 8 (2012) 3314–3321.
[61] H. Gohlke, C. Kiel, D.A. Case, Insights into protein–protein binding by binding free energy calculation and free energy decomposition for the Ras-Raf and Ras–RalGDS complexes, J. Mol. Bio. 330 (2003) 891–913.
[62] M. Khavani, M. Izadyar, M.R. Housaindokht, Theoretical design of the cyclic lipopeptide nanotube as a molecular channel in the lipid bilayer, molecular dynamics and quantum mechanics approach, Phys. Chem. Chem. Phys. 17 (2015) 25536–25549.
[63] M. Izadyar, M. Khavani, M.R. Housaindokht, A combined molecular dynamic, and quantum mechanic study of the solvent and guest molecule effect on the stability and length of heterocyclic peptide nanotubes, Phys. Chem. Chem. Phys. 17 (2015) 11382–11391.
[64] M. Khavani, M. Izadyar, M.R. Housaindokht, Glucose derivatives substitution and cyclic peptide diameter effects on the stability of the self-assembled cyclic peptide nanotubes; a joint QM/MD study, J. Mol. Graph. Model. 71 (2017) 28–39.
[65] J. Carlsson, L. Boukharta, J. Åqvist, Combining docking, molecular dynamics and the linear interaction energy method to predict binding modes and affinities for non-nucleoside inhibitors to HIV-1 reverse transcriptase, J. Med. Chem. 51 (2008) 2648–2656.
[66] K. Moritsugu, T. Terada, A. Kidera, Free-energy landscape of protein–ligand interactions coupled with protein structural changes, J. Phys. Chem. B 121 (2017) 731–740.